

# Modeling the Dynamics of Chromophores in Conjugated Polymers: The Case of Poly(2-methoxy-5-(2'-ethylhexyl)oxy 1,4-phenylene vinylene) (MEH-PPV)

Caroline De Leener,<sup>†</sup> Emmanuelle Hennebicq,<sup>†</sup> Juan-Carlos Sancho-Garcia,<sup>‡</sup> and David Beljonne<sup>\*,†</sup>

Laboratory for Chemistry of Novel Materials, University of Mons-Hainaut, 20 Place du Parc, B-7000 Mons, Belgium, and Departamento de Química Física, Universidad de Alicante, E-03080 Alicante, Spain

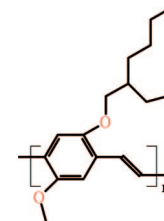
Received: April 7, 2008; Revised Manuscript Received: November 3, 2008

By combining force-field approaches to quantum-chemical techniques, we have explored the influence of conformational changes on the nature of the lowest electronic excitations in model chains of poly(2-methoxy-5-(2'-ethylhexyl)oxy 1,4-phenylene vinylene) (MEH-PPV). The presence of conformational kinks yields a multichromophoric picture for the electronic excitations, where conjugated segments with an average length of ~8 repeat units are delineated by defects. This description applies to both isolated chains and to the bulk material, though very different dynamics are at play. Calculations on interacting polymer chains show that local fluctuations in the density give rise to chains that are on average more planar and thus appear as red sites. These results are discussed in light of recent single molecule spectroscopy data.

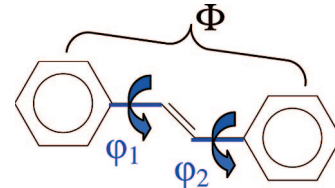
## 1. Introduction

Conjugated polymers combine the optoelectronic properties of semiconductors with the mechanical and processing advantages of plastics. These materials, when functionalized with flexible side groups, become soluble in organic solvents and can be processed from solutions at room temperature into large-area thin films of controlled shape and thickness. That explains why conjugated polymers aroused a considerable interest recently as active materials for promising technological applications, such as electroluminescent diodes, solar cells, or biosensors.<sup>1–3</sup> In the working principle of these devices, the process of electronic excitation migration between conjugated segments making up the polymer chains plays an essential role.<sup>4,5</sup> For instance, polymer-based (bio)chemical sensors are based on a reversible and extremely sensitive quenching of the polymer photoluminescence in the presence of a very small quantity of a target analyte. Compared to the corresponding “small molecules”, conjugated polymers lead to an enhanced sensory response in the presence of one analyte, which has been explained in terms of the collective response of the coupled monomer units.<sup>6,7</sup> To which extent it is the case and what is the mechanism for the energy migration process involved in the quenching mechanism are still open questions.<sup>8</sup> One closely related key issue is the relationship between the conformation of these chains and their electronic structure in the excited state.<sup>9–11</sup> In particular, most of the models applied so far to account for excitation diffusion in conjugated polymers rely on the concept of “chromophores”.<sup>12</sup> Why do these chromophores form and what do they look like is not fully understood yet, but there is compelling evidence for their existence from a large number of experimental investigations. As a matter of fact, a multichromophoric picture for photoinduced electronic excitations in conjugated polymers has been successfully applied to

## SCHEME 1



## SCHEME 2



account for the photophysical behavior of phenylenevinylene-based materials, particularly the line shape and line width of the optical absorption and emission spectra,<sup>13</sup> the observed dispersive-like energy transport,<sup>14</sup> and the intermittent single chain fluorescence.<sup>15</sup> According to this view, energy diffusion proceeds via a hopping mechanism in the energy manifold resulting from the distribution of conjugation lengths and hence excitation energies.<sup>14</sup>

One of the most widely studied and exploited soluble conjugated polymers in plastic electronics is poly(2-methoxy-5-(2'-ethylhexyl)oxy 1,4-phenylene vinylene) (MEH-PPV, see Scheme 1),<sup>8,9,12–16</sup> mostly because of its ease of use and versatility. A large number of spectroscopic investigations have been carried out for this polymer, in the isolated molecules,<sup>14–20</sup> in solution,<sup>21</sup> and on thin films.<sup>21</sup> In MEH-PPV, the formation of chromophores is believed to be driven by the relatively flat conformational potential energy surface and the resulting twists along the backbone disrupting the  $\pi$ -conjugation. MEH-PPV adopts rod-coiled and/or defect cylinder morphologies where the chains fold owing to the presence of chemical (e.g., sp<sup>3</sup>

\* To whom correspondence should be addressed. E-mail: David@averell.umh.ac.be.

<sup>†</sup> University of Mons-Hainaut.

<sup>‡</sup> Universidad de Alicante.

**TABLE 1: Optimized Energetic and Geometric ( $\varphi$ , the Torsion Angles between the Phenyl Rings and the Central Double Bond, See Scheme 2) Parameters for *trans*-Stilbene<sup>a</sup>**

theoretical method	$\varphi_1$ ( $=\varphi_2$ ) (deg)	$\Delta E_{0-30^\circ}$ (kcal/mol)
PCFF (1)	30	0.52
UFF (2)	30	1.37
COMPASS (3)	0	1.11
B3LYP (4)	0	1.37
B3LYP/MP2 (5)	15	0.34
experiment (6)	0–30	

<sup>a</sup> (1) Polymer consistent force field; (2) universal force field; (3) condensed-phase optimized molecular potentials for atomistic simulation studies; (4) density functional theory with the B3LYP functional; (5) density functional theory with the B3LYP functional optimization coupled to an energy calculation with Møller–Plesset perturbation methods at the second order; (6) range of values reported from experimental studies.<sup>38–44</sup>

**TABLE 2: PR Average Values and Standard Deviations in 10-mer and 30-mer MEH-PPV Chains (Isolated Chains and for MEH-PPV<sub>10</sub> in the Bulk); The Fraction of Torsion Defects Is Also Indicated**

	MEH-PPV <sub>10</sub> single chains	MEH-PPV <sub>30</sub> single chains	MEH-PPV <sub>10</sub> bulk
$\langle PR_1 \rangle \pm$ standard deviation	$5.42 \pm 0.90$	$7.62 \pm 3.05$	$4.74 \pm 0.96$
% of torsion defects, $\varphi$	13%	15%	35%
% of torsion defects, $\Phi$	20%	19%	23%
% of torsion defects, total	15%	16%	31%
$\langle \varphi \rangle \pm$ standard deviation	$135 \pm 9^\circ$	$135 \pm 8^\circ$	$136 \pm 2^\circ$
$\langle \Phi \rangle \pm$ standard deviation	$34 \pm 13^\circ$	$34 \pm 7^\circ$	$44 \pm 2^\circ$

atoms) or conformational defects. As a result of polymer folding, segments located far apart along the molecular backbone can be brought in close contacts.<sup>15</sup> Thus, the zero-order electronic structure of MEH-PPV corresponds to an ensemble of chromophores that are (weakly) coupled through-space. Here, the impact of conformational motion on the electronic excited states of MEH-PPV is studied theoretically by combining molecular dynamic simulations of model polymer chains to semiempirical quantum-chemical calculations. Our aim is to identify the possible formation of chromophores resulting from conformational disorder and the associated dynamics for isolated versus interacting chains.

## 2. Theoretical Methodology

Modeling the structural organization of polymer chains requires taking into account several hundreds or even thousands of atoms, which cannot be readily achieved using quantum-chemical approaches. We have thus opted for the classical methods of molecular mechanics and molecular dynamics<sup>22</sup> to explore the conformational potential energy surface (PES) of long MEH-PPV chains. Such an approach is not only affordable from a purely computational point of view but also adapted to the simulation of the intermolecular interactions governing the arrangement of conjugated molecules in the condensed phase. The geometric structures of single MEH-PPV chains consisting of 10 and 30 monomer repeat units have been calculated by combining Monte Carlo (MC) simulations and molecular dynamics (MD) calculations in a fully atomistic representation of the system. The same calculations have been repeated for three chains (each 10 monomer repeating units long) interacting in a periodic cell. We thereby aim at reproducing the interactions between the chains in the “bulk” state, as well as the interactions between different conjugated segments of a long, coiled chain in solution or in an inert polymer matrix. The optical properties of the most stable conformers identified from the MC/MD

simulations have been subsequently calculated on the basis of the semiempirical Hartree–Fock intermediate neglect of differential overlap (INDO) Hamiltonian coupled to a single configuration interaction (SCI) scheme, as parametrized by Zerner and co-workers,<sup>23</sup> in each case, the configuration space involves all of the relevant single excitations between molecular orbitals (a total of 40 MOs for the 10-unit chains and 120 MOs for the 30-unit chains was used).

The molecular mechanics computations presented in this work have been carried out using the 4.0 version of Cerius2<sup>24</sup> and the 4.0 version of Material Studio<sup>25</sup> programs and the standard PCFF, UFF, and COMPASS force fields that are provided in these packages. All of these simulations were done at 300 K with a Hoover thermostat and using a spline curve from 11 to 14 Å in the description of the nonbonded interaction terms. For each MEH-PPV<sub>10</sub> and MEH-PPV<sub>30</sub> isolated chain, two Monte Carlo simulations were first performed to generate randomly 5000 probable conformations. The most stable MC structures were used as a starting point in three molecular dynamics simulations at constant NVT (for 500 ps in the 10-mer and 1 ns in the 30-mer), out of which the five lowest conformers were extracted for subsequent analysis (hence, a total of 15 structures were examined for both chains). The same kind of MD procedure has been applied in the case of interacting molecules. There, cubic periodic boxes of 20 Å size including three chains of 10 monomer repeat units are generated to yield a density of ~1 g/cm<sup>3</sup>. To equilibrate the system, we performed successive MD simulations at 600, 550, 500, 450, 400, and 350 K; a MD simulation of 1 ns at 300 K was then run to explore the potential energy surface. In both cases (isolated molecules and bulk phase), the geometric structures are extracted as snapshots along the MD trajectories and fully optimized by means of the conjugate gradient method, a first-derivative technique.

All *ab initio* (MP2, DFT<sup>26</sup>) calculations were carried out using the Gaussian 03 package.<sup>27</sup> Density functional theory<sup>26</sup> employing the hybrid Becke three-parameter Lee–Yang–Parr (B3LYP) functional has been shown to be a very powerful theoretical method for describing ground-state geometries.<sup>28–35</sup> However, these calculations based on exchange-correlation functionals usually describe only poorly long-range nonbonding interactions.<sup>28,34–38</sup> Thus, in order to evaluate the influence of electron correlation effects on the shape of the ground-state PES, single point energy calculations have been performed at the MP2 level on the basis of the B3LYP/cc-pVDZ geometries.<sup>28,38–40</sup>

## 3. Results and Discussion

### 3.1. Selection of a Force Field: The Case of Stilbene.

To assess the accuracy of various force fields in describing the conformation of MEH-PPV chains, we have focused on the ground-state potential energy surface (PES) of *trans*-stilbene (Scheme 2), the shortest oligomer representative of PPV and its derivatives. The ground-state geometry of *trans*-stilbene has been calculated by means of the molecular mechanics PCFF, UFF, and COMPASS force fields<sup>41,42</sup> and compared against quantum-chemical data in order to test the capability of force-field techniques to reproduce the equilibrium geometric structures of the local minima on the PES and their relative energies (see Table 1).

Among the force fields tested, PCFF yields ground-state geometric and energetic parameters that compare well with the results of the combined DFT/MP2 calculations. In particular, both approaches lead to a global minimum for torsion angles between the phenyl rings and the central double bond  $\varphi$  on the order of ~±30°. The PES is very flat around the minimum:

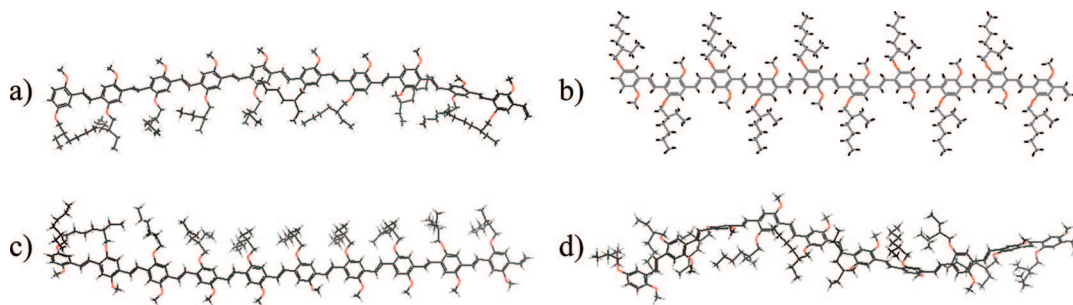


**Figure 1.** Conformation of two representative MEH-PPV<sub>10</sub> chains: (a) stable structure generated by MC simulations; (b) planar structure with the bulky side groups alternated along the backbone. Most stable conformers for MEH-PPV<sub>10</sub> chains generated from MD simulations: (c) ethylhexyloxy groups on the same side of the backbone with average torsion angle,  $\varphi$ , around C–C single bonds of 30–35°; (d) ethylhexyloxy groups on both sides of the backbone with slightly larger average  $\varphi$  values of 35–40°.

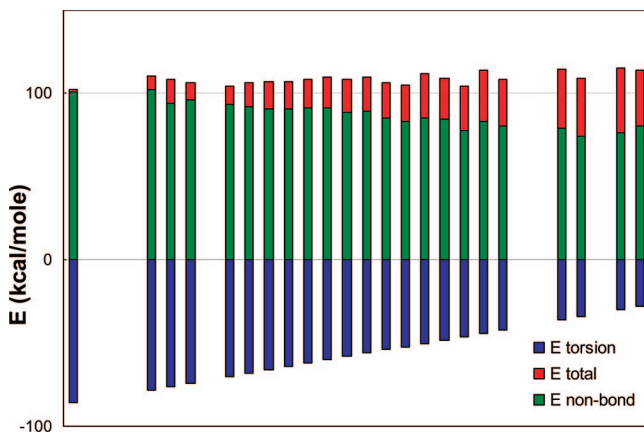


**Figure 2.** Torsion and nonbonding contributions (in kcal/mol) to the total energy of the 100 most stable MEH-PPV<sub>10</sub> chains generated from a total of six MD simulations. The line at energy = 100 kcal/mol is a guide to the eye.

the energy difference between the planar and twisted conformers amounts to 0.52 kcal/mol at the PCFF level, in good agreement with the DFT/MP2 result of 0.34 kcal/mol.

On the experimental side, it has been suggested that conformations corresponding to values of the dihedral angle  $\varphi$  ranging from  $-30$  to  $30^\circ$  are all statistically probable in *trans*-stilbene, due to the flatness of the potential energy surface. Torsion angles of  $30$  and  $32^\circ$  were inferred from gas-phase electron diffraction experiments performed at  $200$  and  $280\text{ }^\circ\text{C}$ , respectively.<sup>43</sup> At room temperature<sup>44–46</sup> and at  $-160\text{ }^\circ\text{C}$ ,<sup>47</sup> torsion angles  $\varphi$

ranging from  $0$  to about  $7^\circ$  are reported from X-ray diffraction studies of *trans*-stilbene crystals in the solid phase. Compared to the gas phase, the flattening of the molecule in the condensed phase clearly results from packing effects and  $\pi$ – $\pi$  interactions. Analysis of the vibronic structure observed in the  $\pi$ – $\pi^*$  fluorescence spectrum of a crystalline stilbene sample at  $20\text{ K}$  suggests torsion angles approaching  $10^\circ$ .<sup>48</sup> Moreover, deviations from planarity until  $30^\circ$  have been suggested as a result of thermal disorder from a joint theoretical and experimental study.<sup>49</sup>

**3.2. MEH-PPV Isolated Chains. 3.2.1. Ground-State Conformation Analysis.** The conformational study of MEH-PPV chains, including  $10$  (MEH-PPV<sub>10</sub>) and  $30$  (MEH-PPV<sub>30</sub>) monomer repeat units, has been carried out by means of Monte Carlo (MC) and molecular dynamics (MD) simulations as detailed in section 2. These allow exploring the potential energy surface and unraveling the most stable conformers. Three MD simulations have been run using the most stable conformers generated from MC simulations as initial structures (see Figure 1a); in addition, we also performed MD simulations assuming as starting structure a planar conformation where all of the ethylhexyloxy substituents are perfectly alternated on each side of the backbone as a starting point (see Figure 1b).

At the end of each MD simulation, the five most stable structures were selected and fully optimized. Two types of structures with similar total energies have been identified from these calculations. In the first group, most of the ethylhexyloxy substituents lie on the same side of the backbone (Figure 1c); this translates into torsion angles  $\varphi$  of  $\sim 30$ – $35^\circ$  around the

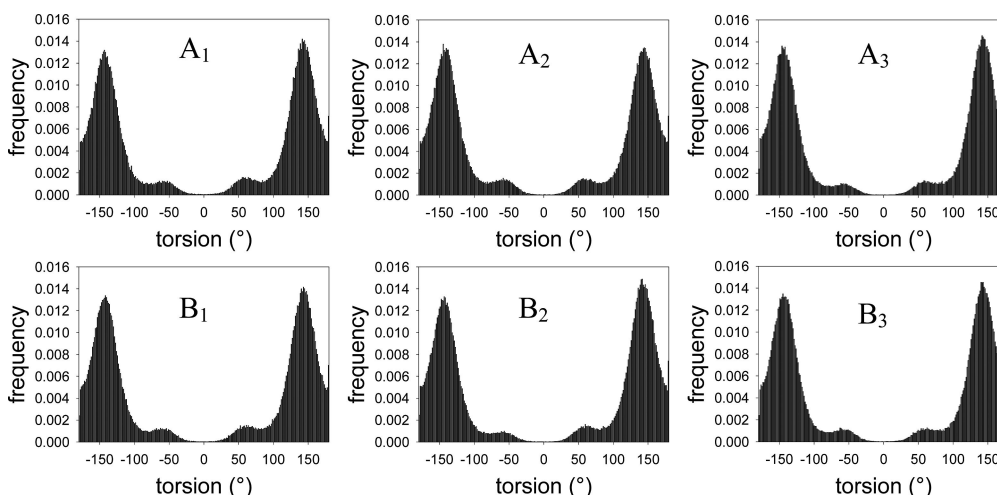


**Figure 3.** Distribution of the torsion angles,  $\varphi$ , for six MD simulations of MEH-PPV<sub>30</sub> chains as initial structures: conformation a ( $A_1$ ,  $A_2$ ,  $A_3$ ) and conformation b ( $B_1$ ,  $B_2$ ,  $B_3$ ) of Figure 1.

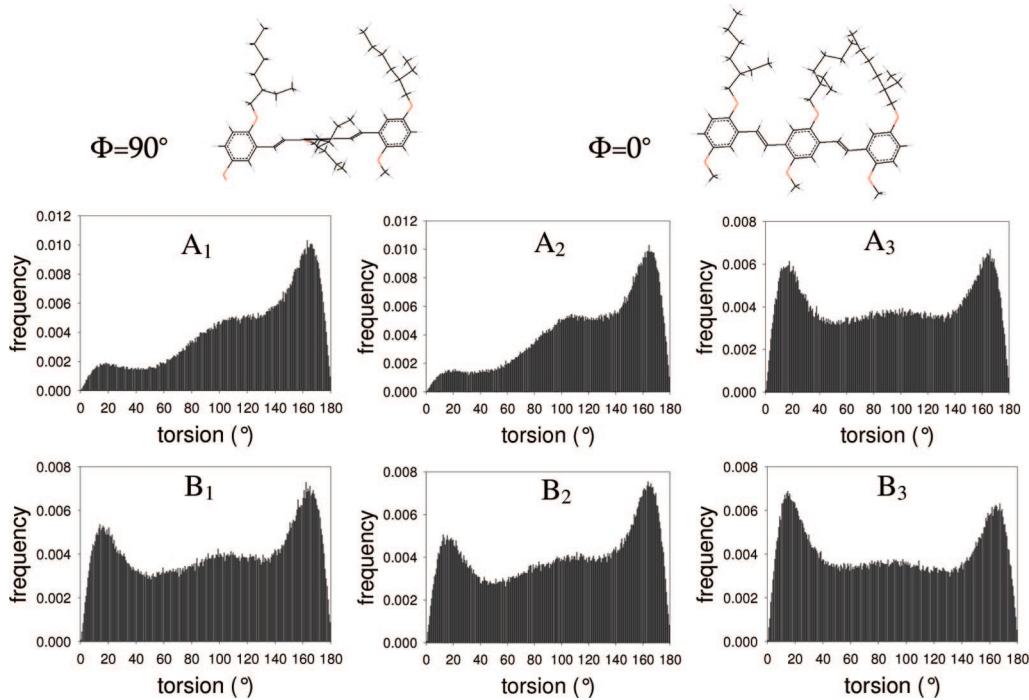


**Figure 4.** Distribution of torsion angles,  $\Phi$ , between two successive phenyl rings for six MD simulations of MEH-PPV<sub>30</sub> chains as initial structures: conformation a (A<sub>1</sub>, A<sub>2</sub>, A<sub>3</sub>) and conformation b (B<sub>1</sub>, B<sub>2</sub>, B<sub>3</sub>) of Figure 1. For the sake of illustration, two limiting cases for successive rotations around vinylene single bonds ( $\Phi = 0^\circ$  and  $\Phi = 90^\circ$ ) are shown on top for a three-unit oligomer.

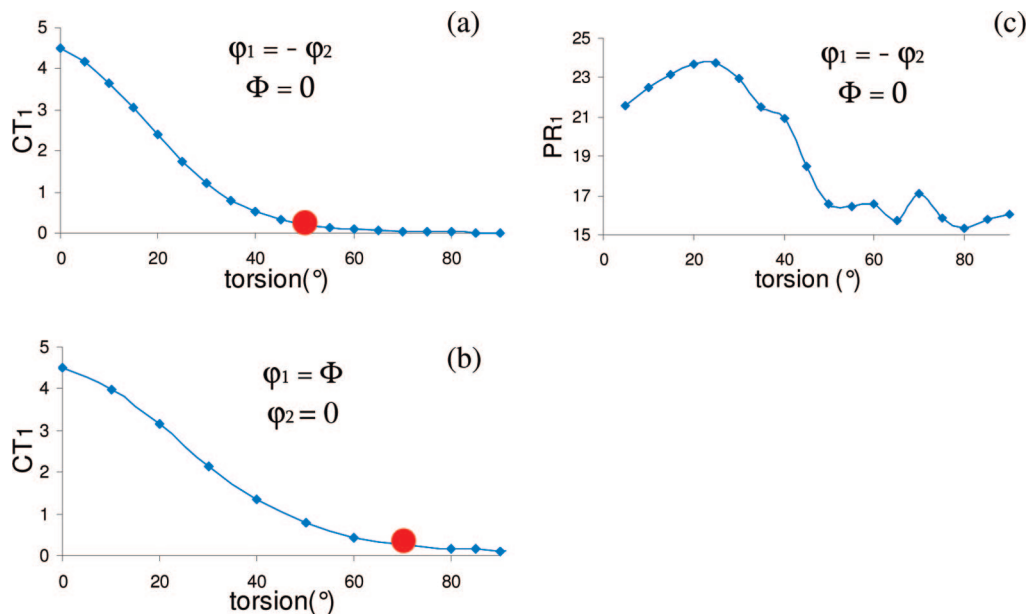


**Figure 5.** Influence of a central twist kink on the degree of conjugation in a 30-unit PPV chain: as measured by the charge-transfer character (a and b) between the two conjugated segments separated by the defect and as measured by the participation ratio (c) in the lowest excited state of a 30-unit chain.

C–C single bonds of the vinylene units. In the second ensemble of conformers (Figure 1d), the ethylhexyloxy substituents are randomly positioned around the backbone with, as a result, a slight increase in the torsion angles  $\varphi$  (35–40°). These two sets of conformers display similar potential energies: Compared to the first group, chains belonging to the second group are stabilized by more favorable nonbonded interactions (on average by ~16 kcal/mol) but destabilized by the torsion contribution (by about the same amount). The relevant contributions to the total energy are illustrated in Figure 2 for 100 conformers generated.

We now analyze in more detail the conformation of the chains generated along the MD simulations. The torsion angles around

the vinylene single C–C bonds,  $\varphi$ , have a major impact on the amount of excitation delocalization, as described in the next section and displayed in Figure 3. It is also instructive to follow the angle between the planes defined by successive phenyl rings,  $\Phi$  (see Figure 4), as it allows identifying the presence of conjugation breaks. Note that  $\Phi = \varphi_1 + \varphi_2$ , where  $\varphi_1$  and  $\varphi_2$  are the torsion angles around the two carbon–carbon single bonds comprised between two successive phenyl rings, Scheme 2. The distributions reported in Figures 3 and 4 are obtained by collecting all torsions along a 30-unit MEH-PPV chain at each step of the MD runs. Similar results are obtained for MEH-PPV<sub>10</sub> chains. The most stable conformations ensure a compromise between the energy gain associated with delocalization

of the  $\pi$  electrons along the chain and the steric repulsion between the alkoxy side groups. From Figure 3, the resulting torsion angles around the single C–C bonds of the vinylene units,  $\varphi$ , oscillate around  $\pm 45$  and  $\pm 135^\circ$ . Accordingly, four peaks can be distinguished on each histogram; the presence of two doublets with almost symmetric weights is due to the two possible rotation signs around the C–C single bond, while the doublet itself (with a high- and a low-probability peak) comes about from the different orientations of the vinylene double bond and the alkoxy side chains on the neighbor phenyl rings; see Scheme 3. The smaller population associated with the  $\pm 45^\circ$  peaks can be rationalized on the basis of the steric effects between the alkoxy substituents and the closest hydrogen atoms of the neighboring vinylene linkage, Scheme 3.

The histograms for the torsion angles,  $\Phi$ , between two successive rings show three broad features centered around 20, 90, and  $160^\circ$ . Thus, depending on whether two successive rotations around the C–C single bonds occur in-phase or out-of-phase, the phenyl aromatic rings will be either in an almost coplanar conjugation or in a perpendicular arrangement. As can be easily anticipated, the degree of conjugation along the chains will be very significantly affected not only by the amplitude of these torsions but also by their sequence.

**3.2.2. Excited-State Electronic Structure Analysis.** On the basis of the ground-state geometric structures generated by the MD simulations, we have applied semiempirical quantum-chemical techniques (INDO/SCI) to study the influence of conformational fluctuations on the nature and spatial extent of the lowest electronic excited states in chains ranging in size from 10 to 30 units. The degree of delocalization in the  $n$ th singlet excited state  $S_n$  can be evaluated by partitioning the two-particle excited-state wave function into local,  $|\psi_i\rangle$ , and charge-transfer,  $|\psi_{ij}\rangle$ , configurations (where  $i$  and  $j$  denote different repeating units):

$$|\psi_n\rangle = \sum_i c_{n,i} |\phi_i\rangle + \sum_i \sum_{j \neq i} c_{n,i-j} |\phi_{i,j}\rangle \quad (1)$$

The overall contribution from monomer unit  $i$  to the excited-state wave function is then calculated as<sup>50</sup>

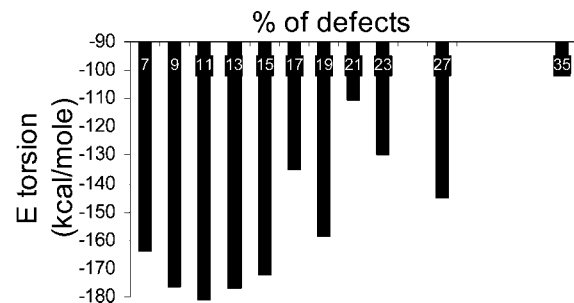
$$b_{n,i}^2 = c_{n,i}^2 + \frac{1}{2} \sum_{j \neq i} c_{n,i-j}^2 \quad (2)$$

From this, we define the participation ratio for excited state  $S_n$  as

$$\text{PR}_n = \frac{\sum_{i=1}^N b_{n,i}^2}{\sum_{i=1}^N b_{n,i}^4} \quad (3)$$

$\text{PR}_n$  can be regarded as the number of sites coherently coupled in the excited state  $S_n$ .<sup>51</sup> It is also useful to define the charge-transfer ( $\text{CT}_n$ ) character between two segments  $s_1$  and  $s_2$  of the polymer chain, as calculated in the  $S_n$  singlet excited state by

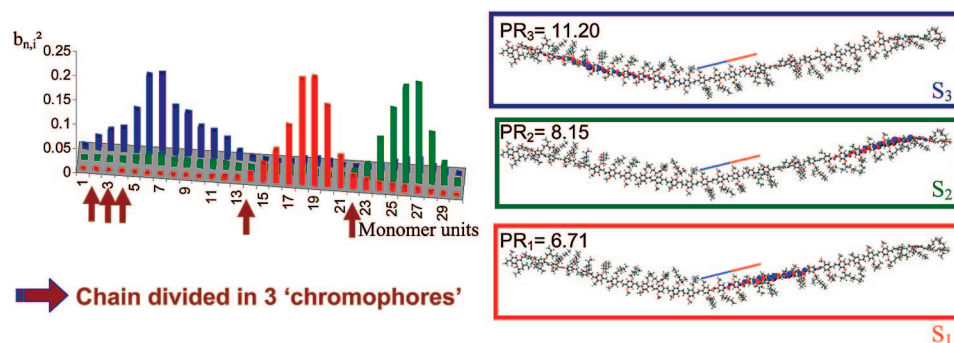
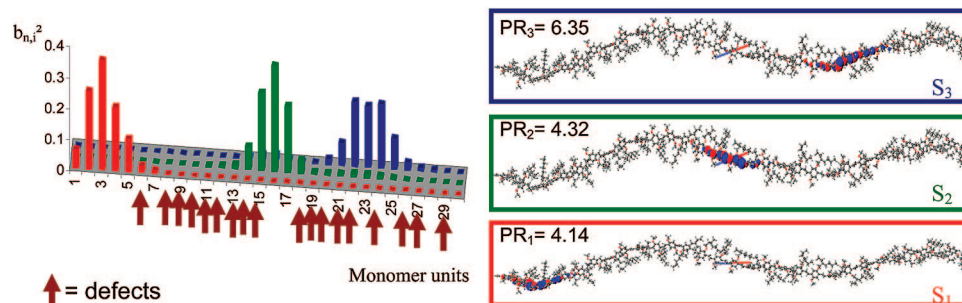
$$\text{CT}_{n,s_1 \rightarrow s_2} = \sum_{i \in s_1} \sum_{j \in s_2} c_{n,i-j}^2 \quad (4)$$



**Figure 6.** Torsion contribution to the potential energy as a function of the concentration of torsion defects in MEH-PPV<sub>30</sub> chains. The defect concentration is normalized to the total number of torsion angles along the chains (i.e., a total of 88 torsion angles).

In order to assess the influence on the conjugation along the chain of deviations from planarity, we have calculated the CT character in the lowest singlet excited state of a PPV<sub>30</sub> chain that contains a single torsion kink in its center; thus, the chain consists of two fully planar conjugated segments connected by a central vinylene linkage with C–C torsion angles ranging from  $\varphi_1 = 0^\circ$  to  $\varphi_1 = 90^\circ$  (and  $\varphi_2 = -\varphi_1$ , so that  $\Phi = 0$ ), Figure 5a. As expected from the reduced wave function overlap, the CT character between the two segments decreases with increasing torsion angle and reaches 0 for  $\varphi_1 = -\varphi_2 = 90^\circ$ . Above  $\sim 50^\circ$ , CT<sub>1</sub> has decayed to 10% of its value in the fully planar configuration, which is hereafter associated with a conjugation break. As the same evolution is observed in the range  $\varphi_1 = 90-180^\circ$ , a torsion angle  $\varphi$  between adjacent phenyl rings comprised between 50 and  $130^\circ$  is counted as a torsion defect disrupting the conjugation. Applying the same criterion for rotations between adjacent phenyl rings  $\Phi = \varphi_1 (\varphi_2 = 0)$  yields a cutoff of  $70^\circ < \Phi < 110^\circ$  for a conjugation defect, Figure 5b.

In the absence of defects (i.e., planar conformation), the excitation delocalizes over the entire chain and PR<sub>1</sub>, defined in eq 3, reaches a maximum value of  $\sim 21$ . This is slightly smaller than the full length of the chain (30) as a result of finite size effects. Fidder et al. show that, for a perfect chain and retaining only nearest neighbor interactions, PR for the lowest excited state should scale as  $2(N + 1)/3$  in the limit of complete delocalization.<sup>51</sup> For  $N = 30$ , this translates into a maximum PR value of  $62/3 \approx 20$ , i.e., close to the INDO/SCI value. The evolution of PR<sub>1</sub> with the torsion angles around the two most central C–C vinylene bonds (with  $\varphi_2 = -\varphi_1$ ) portrayed in Figure 5c complies with the analysis performed on the basis of the charge-transfer character (Figure 5a and b): PR<sub>1</sub> decreases with  $\varphi_1$  to reach the value of  $\sim N/2 (=15)$  for  $\varphi_1 \geq 50^\circ$ . For such large torsion angles, the excitation is thus almost completely localized on a single segment. However, the evolution of PR<sub>1</sub> with the amount of twisting is somewhat more chaotic than that of CT<sub>1</sub> and shows an initial increase for  $\varphi_1 \in [0-40^\circ]$ . In fact, even in the case where the conjugation is completely broken (no *through-bond* interactions), the excited-state wave function can still spread over the two subconformers via *through-space* couplings. As these are weak dipole–dipole interactions, they are only effective in delocalizing the electronic excitation in the case of close degeneracy between the electronic structure of the two separate chromophores. While such degeneracy effects play a role in the case of the model bichromophoric systems of Figure 5 (thereby explaining the nonmonotonous evolution of PR<sub>1</sub>, with  $\varphi_1$ ), they are only fortuitous in the polymer chains generated from the MD simulations owing to the significant conformational and thus energetic disorder.

Chain A (6 conformational defects):  $\langle PR \rangle = 8.7$ Chain B (32 conformational defects):  $\langle PR \rangle = 4.9$ 

**Figure 7.** Mapping of the electronic transition density associated with the lowest three electronic excitations onto the repeating units of two different conformations of MEH-PPV<sub>30</sub> chains.

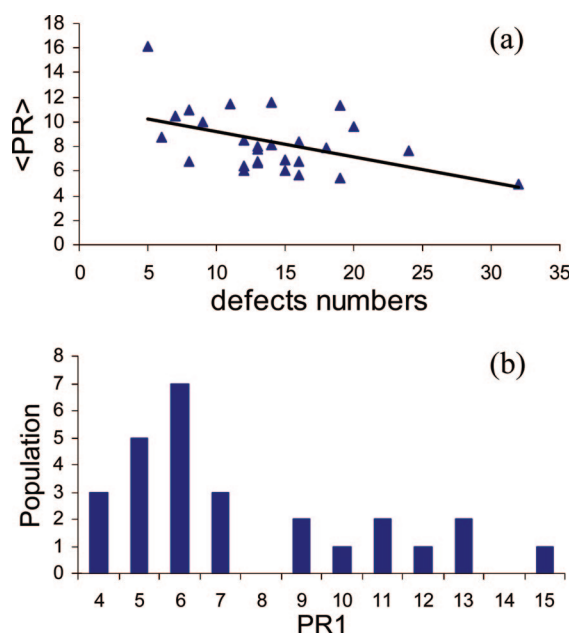


**Figure 8.** (a) Correlation between the number of torsion kinks and the average PR. (b) Histogram of conjugation lengths as measured by the participation ratio in 30-mer MEH-PPV isolated chains.

On the basis of the criteria defined above for  $\varphi_1$  and  $\Phi$ , a fraction of conformation kinks of 16% has been extracted from the conformational analysis of the 30 most stable conformers generated by MD simulations for MEH-PPV<sub>10</sub> and MEH-PPV<sub>30</sub> chains (see Table 2). Figure 6 shows that the torsion energy penalty associated with the presence of such conformational kinks is limited for concentration of “defects” lower than ~15% and is partly compensated by interactions between side chains.

We now move to the discussion of the localization of the electronic excitations induced by the presence of conformational defects. As it turns out that the calculated average conjugation length in MEH-PPV is slightly smaller than 10, we have registered the PR values calculated for the lowest three singlet excited states of the 30 MEH-PPV<sub>30</sub> chains (that localize on three distinct subunits of the chain). These calculations clearly suggest that the conformational kinks identified above lead to a partitioning of the chain into finite conjugated segments and allow quantifying the length of the resulting chromophores. As an illustration, we portray in Figure 7 the excited-state wave function localization (as represented by transition density maps) obtained for two MEH-PPV<sub>30</sub> chains generated from the initial structures a and b of Figure 1. The arrows on the figure indicate torsional defects on the chains. Note that these chains have similar total energy and belong to the two types of structures discussed previously (Figure 1). They include 6 and 32 torsional defects and feature an average PR value for the lowest three excited states of 8.7 and 4.9, respectively. Thus, the polymer chains are chopped into chromophores, whose length is fixed by the number of torsional defects. This is better illustrated in Figure 8a, highlighting the correlation between the amount of excited-state delocalization as measured by the PR and the number of torsion-induced conjugation defects. By averaging over all chains generated, mean delocalization lengths of 5.4 and 7.6 are found in 10-mer and 30-mer chains. Though the number of chains investigated here does not allow for a statistical analysis, we stress that the PR distribution is asymmetric with a long tail extending to large PR values (up to 15). Note that the slightly smaller value obtained for MEH-PPV<sub>10</sub> is due to finite size effects.

To conclude this section, isolated MEH-PPV chains are composed of conformational subunits with an average conjuga-

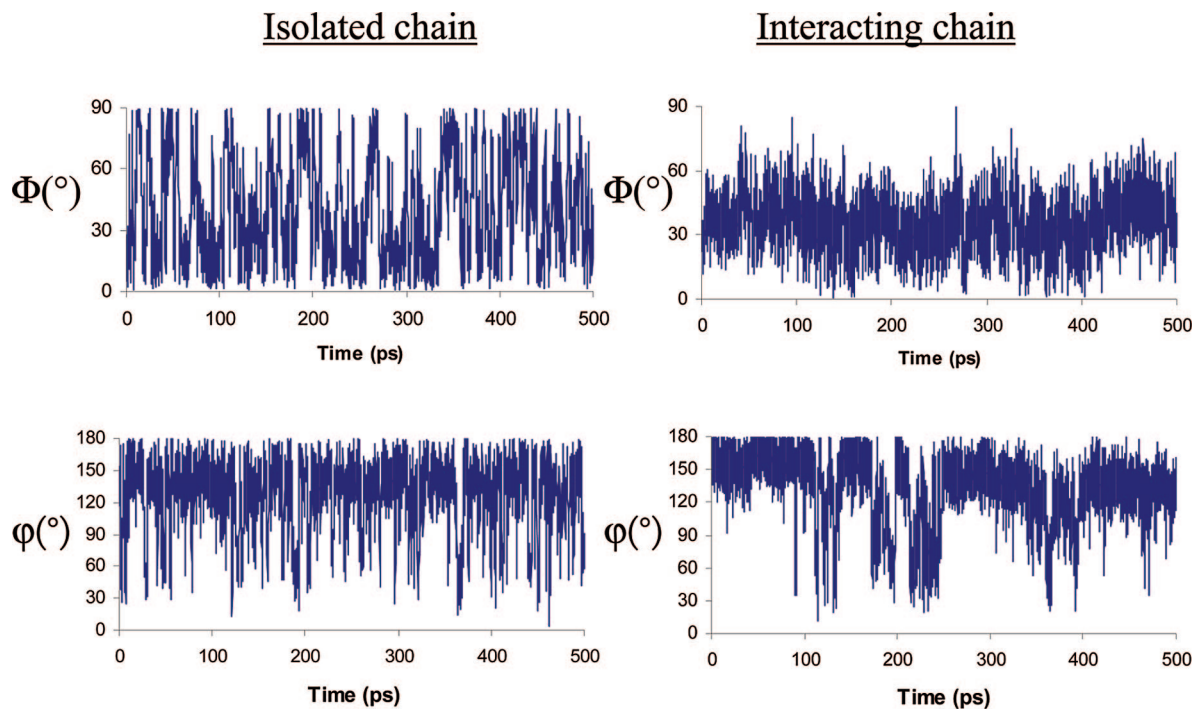


**Figure 9.** Time evolution of the torsion angles  $\varphi$  and  $\Phi$  around the center of a 10-unit MEH-PPV chain in the gas phase (left) and in the bulk (right).

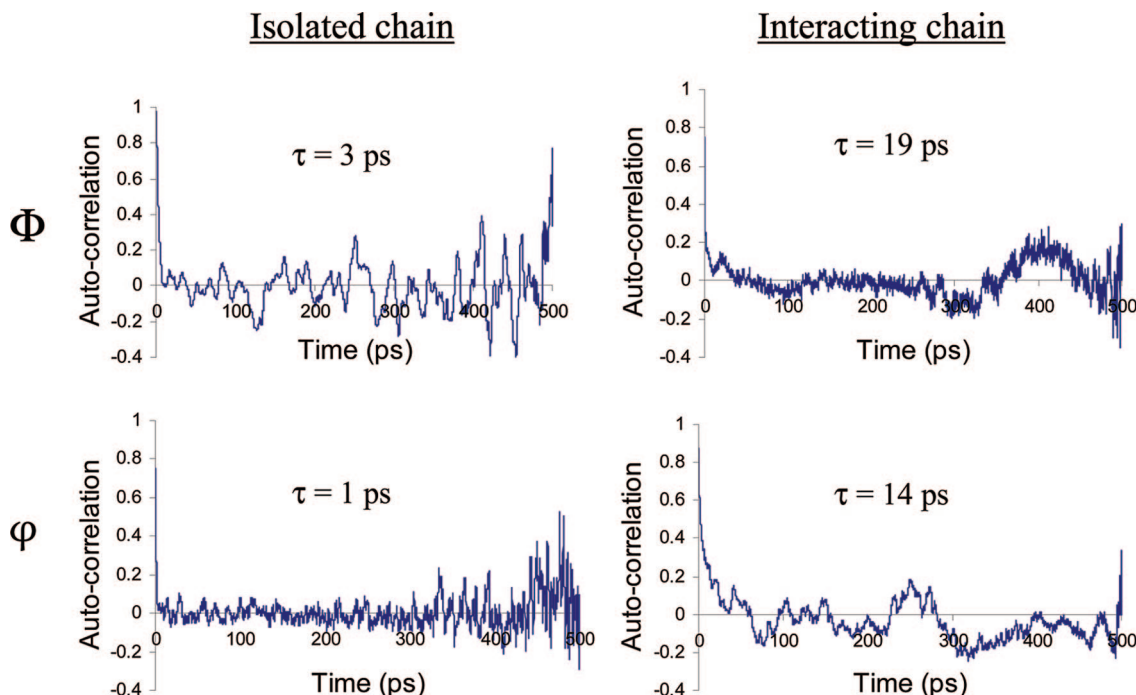


**Figure 10.** Autocorrelation function of torsion angles  $\varphi$ ,  $\langle \varphi(t) \varphi(0) \rangle$ , and  $\Phi$ ,  $\langle \Phi(t) \Phi(0) \rangle$ , around the center of a 10-unit MEH-PPV chain in the gas phase (left) and in the bulk (right). The falloff parameters,  $\tau$ , extracted by fitting the first 50 ps with a monoexponential decay law,  $y(t) = a \cdot e^{-t/\tau}$ , are also indicated.

tion length of  $\sim 8$  repeating units. Very similar conclusions have been drawn from a similar quantum-chemical study atop classical molecular dynamic simulations of unsubstituted PPV, yielding a conjugation length in the range 6–12 monomer units.<sup>52</sup> The calculated coherent size of the electronic excitations is also in good agreement yet slightly smaller than single molecule fluorescence spectroscopy data, indicating that the lowest energy optical absorption of isolated MEH-PPV molecules (with  $\sim 1700$  repeat units) involves about 140 different local “quasi-chromophores” along the chains with an average

conjugation length of  $\sim 10$ –17 monomer repeat units.<sup>15–18</sup> Also, the measured optical absorption spectrum of an alkoxy-substituted PPV derivative in solution superimposes almost exactly with that of the corresponding 9- and 11-unit oligomers, suggesting a conjugation length of  $\sim 10$  monomer units.<sup>53</sup> It should be stressed that conjugated polymers are dynamic objects characterized by conformational fluctuations over time scales that depend on their chemical nature as well as their environment. For the sake of illustration, we present in Figure 9 the time evolution of a few representative torsion angles along a

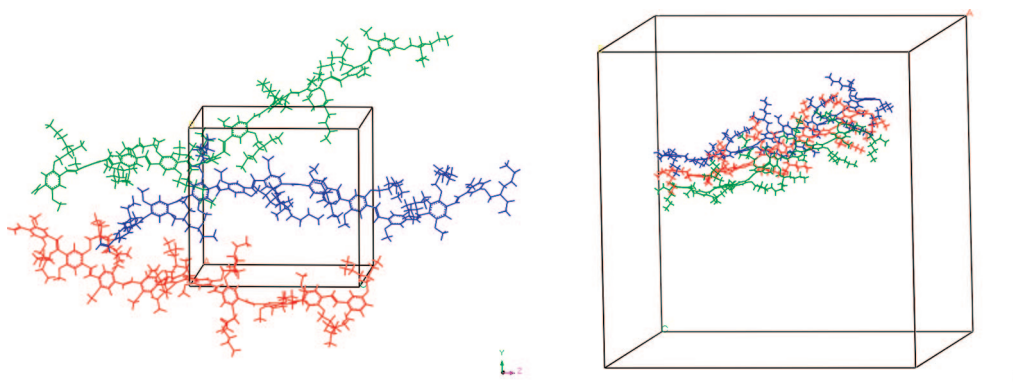


**Figure 11.** Periodic box including three chains of 10 repeating units each with a density of  $1 \text{ g/cm}^3$  (left) and  $0.03 \text{ g/cm}^3$  (right).

10-unit MEH-PPV chain as probed by MD simulations at room temperature; the corresponding autocorrelation functions are displayed in Figure 10. In the gas phase, the molecule explores a large portion of the ground-state potential energy surface within a few picoseconds only, with the torsion angles  $\varphi$  fluctuating around their equilibrium values and the angles  $\Phi$  switching back and forth from the almost coplanar to the near-orthogonal configuration. The corresponding normalized autocorrelation functions  $\langle \varphi(t) \varphi(0) \rangle$  and  $\langle \Phi(t) \Phi(0) \rangle$  drop quickly to zero, indicative of very short memory effects (Figure 10). It is the uncorrelated conformational motion of the different repeating units along the polymer chains that drives the localization of the electronic excitations. As a matter of fact, PR<sub>1</sub> is almost insensitive to large deviations from planarity, provided all torsion angles along the chain are incremented in a simultaneous way; see Table 3. Of course, the charge-transfer character decreases with increasing torsion angles, as displayed in Figure 5, because of reduced wave function overlap. Hence, chains with on average larger torsion angles are more susceptible to break up into conformational subunits in the presence of energetic disorder.

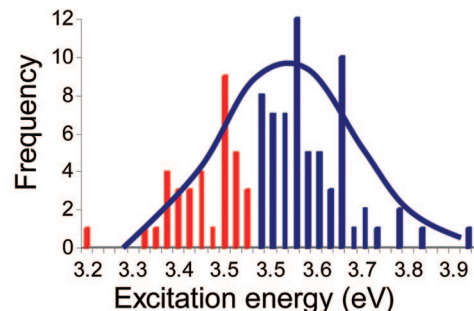
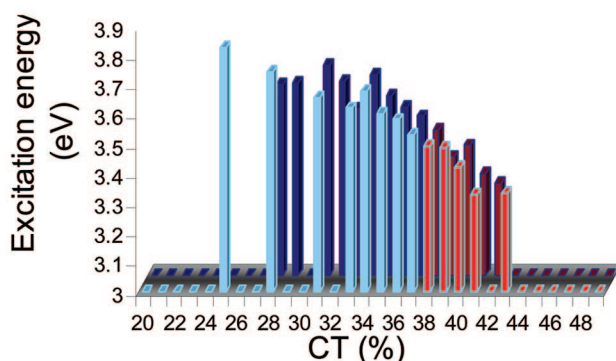
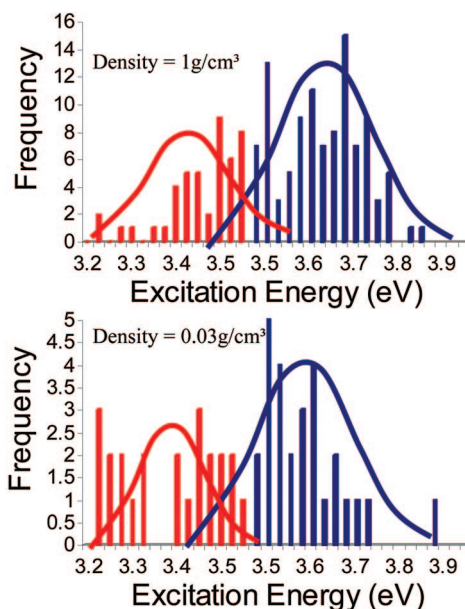
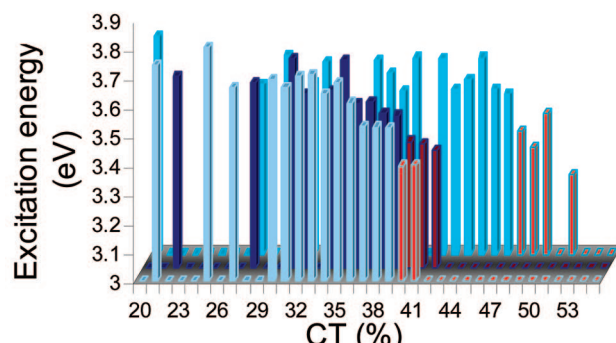
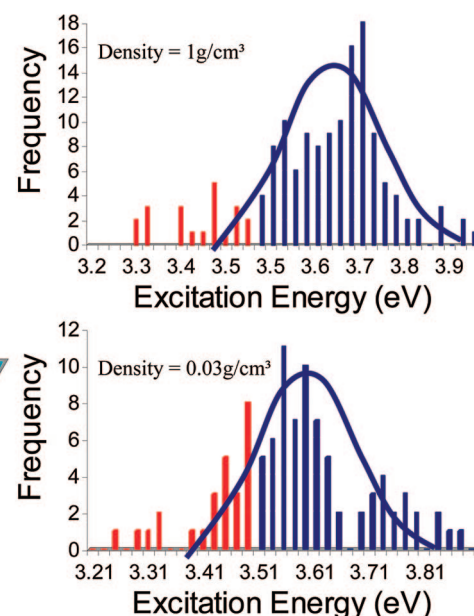
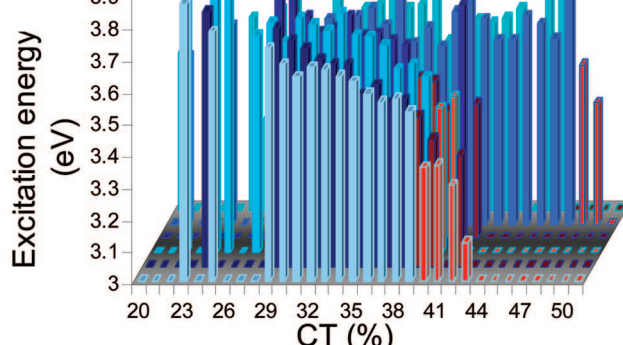
**3.3. MEH-PPV in the Bulk.** All results discussed so far correspond to calculations performed for isolated molecules. We conjecture that these are representative of the behavior in diluted nonviscous solvents. Preliminary calculations performed on MEH-PPV chains embedded in an acetonitrile environment (not shown) confirm this hypothesis. It can be expected that the environment of the polymer chains will influence the conformation of the polymer chains and their dynamics. Recent single molecule spectroscopic studies on long ( $\sim 1700$  monomer repeat units) isolated chains of MEH-PPV are consistent with a multichromophoric picture with the photoinduced electronic excitations funneling into a limited number of low-energy sites where light emission takes place. The origin for these “red” sites was interpreted as a result of folding of the chains on themselves, thereby allowing for interactions between conjugated segments that are brought in close proximity.

To assess the impact of interchromophore interactions on the nature of the lowest electronic excitations, we have built periodic boxes of  $20 \text{ \AA}$  sideways (with a density of  $1 \text{ g/cm}^3$ ) including three chains of 10 monomer repeat units each, Figure 11a. We note that this is representative of the bulk material but should also account in a realistic way for the interactions between segments taking place in coiled single polymer chains. Applying the same methodology as that adopted for isolated molecules (i.e., performing INDO/SCI excited-state calculations on snapshot structures extracted from the MD simulations), we obtain an averaged conjugation length of 5.6 monomer repeat units, very close to the value (5.4) calculated in the gas phase. As

described above, this value is affected by finite size effects and, in view of the similarity between gas-phase and bulk results, we expect the polymer limit to be close to  $\sim 8$  repeating units in the bulk material, as was found for the single MEH-PPV<sub>30</sub> chains. Thus, the concept of chopping the polymer chains into conjugated segments owing to conformational defects is preserved in the bulk. We further note that a larger fraction of torsion defects is predicted in this case (30% as compared to 16% for isolated chains), which likely results from additional steric constraints induced by packing effects.

The average torsion angles  $\varphi$  and  $\Phi$  in the bulk are similar, yet slightly larger than the corresponding values for the isolated chains (Table 2), which is at odds with the commonly accepted dogma that packing effects favor more planar conformations. This likely arises because of structural disorder brought in by the asymmetric alkyl side chains. As expected, the conformational dynamics is very different for interacting versus noninteracting chains, Figure 9. Compared to the isolated chain case,  $\Phi$  and  $\varphi$  show indeed a much slower time evolution, as best pictured by their autocorrelation function decaying to zero within 59 and 35 ps (to be compared to 10 and 11 ps for isolated chains in Figure 10). Fitting these autocorrelation functions over the first 50 ps with an exponential decay function  $y = ae^{-t/\tau}$  yields a decay time for  $\Phi$  and  $\varphi$  of 19 and 14 ps, respectively, in the bulk to be compared to 3 and 1 ps for isolated chains. The difference between the gas and bulk phases is particularly pronounced for the torsion angle between successive phenyl rings, which bounces very quickly between the two minima at  $\sim 0$  and  $\sim 90^\circ$  in a single polymer chain but fluctuates only weakly around its initial value in the bulk. Indeed, large changes in  $\Phi$  are prohibited for interacting chains, as these would require a profound reorganization of the side chains.

Another question that arises at this stage is the relative contributions to the overall excited-state delocalization of the interactions among repeating units belonging to the same chain as compared to distinct chains. In other words, do the electronic excitations significantly spread out over nonbonded neighbor chromophores due to  $\pi$  stacking? The answer is no. For all generated structures, we find that the lowest singlet excited state is confined on a single chain. Thus, the electronic coupling mediating excitation delocalization is not large enough to compete with the pronounced energetic and torsional disorder in MEH-PPV. This is not really surprising, as the chemical structure of the polymer, with branched alkyl chains and asymmetric substitution, has been designed with the purpose of avoiding aggregation-induced quenching of the luminescence. We stress, however, that higher lying excited states within the broad density of states display a more delocalized character.<sup>52,54</sup>

Isolated molecules :Interacting molecules: high local densityInteracting molecules: low local density

**Figure 12.** Population histograms of the first transition energy (right) and correlation between the excitation energy and the amount of conjugation as measured by the CT character (left). The results are given for isolated chains (top) and periodic boxes with either high or low total densities (middle and bottom). For the bulk, chains experiencing high *local* density (middle) behave differently from chains experiencing low *local* density (bottom).

We now come back to the interpretation of the MEH-PPV single molecule spectra. Our calculations indicate that the

presence of red sites cannot be accounted for by the delocalization of the electronic excitations between different conjugated

## SCHEME 3



**TABLE 3: PR<sub>1</sub> Values and Charge-Transfer Character in the Lowest Excited State of a 30-mer PPV Chain Where All φ Torsion Angles Are Incremented in a Simultaneous Way**

φ (deg)	0	10	20	30	40	50	60
PR <sub>1</sub>	20.97	21.19	21.15	21.19	21.08	20.74	20.81
CT (%)	51.0	50.5	49.4	47.5	44.8	41.6	34.0

segments. The analysis of the vertical transition energies computed for geometric structures generated along MD runs in the bulk shows that these follow a different distribution than that found for isolated chains, Figure 12. In the latter case, the excitation energies are spread out around a mean value according to a monomodal distribution. The different energies reflect directly the conformation of the polymer chains, with more planar structures leading to lower transition energies, and chains including many conformational defects featuring higher transition energies, Figure 13. Some of the bulk chains obey a similar pattern, yet with a slight overall blue shift owing to the on average larger torsion angles and larger fraction of conformational kinks, *vide supra*. Others, however, display a significantly different distribution of populations with the appearance of a smaller massif at lower energy. It turns out that chains showing such bimodal distributions systematically arise from regions of the amorphous structure where the local density is higher. In fact, packing effects in the solid yield conjugated segments that have locally a more planar conformation. These have therefore a higher CT character and, as a consequence, feature lower excitation energies. To make sure this effect can be correlated to the packing density, the same calculations were reported for a low-density box (0.003 g/cm<sup>3</sup>); see Figure 11. The same results are obtained when focusing on the chains in the center of the box for which the local density is close to 1 g/cm<sup>3</sup> (Figure 12). However, the red tail in the distribution disappears for the outer chains that experience a lower density environment, thereby confirming the central role of the local packing on the exciton energy distribution. On that basis, we tentatively propose an alternative scenario to explain the red sites observed at the single molecule level in MEH-PPV. According to our calculations, these species indeed originate from packing effects, as was first

suggested, but their lower energy is due to local constraints on the conformation leading to more planar subunits rather than direct excitonic delocalization around chromophores brought in close proximity by chain folding.

## 4. Conclusions

In this paper, we have presented a detailed analysis of the relationships between the conformational disorder in MEH-PPV and the electronic structure in the excited states. We have applied a combined molecular dynamics/quantum-chemistry approach to isolated chains comprising 10 and 30 monomer repeat units as well as to the bulk phase (interacting chains of 10 monomer repeat units). The conformational study reveals important differences in the dynamics of the isolated molecules vs interacting chains. Although the average torsion angles are similar, they experience fluctuations over different time scales. For isolated chains, the different torsion angles along the main backbone vary independently of each other on the time scales of a few picoseconds. The resulting stochastic distribution in torsion angles results in the formation of conjugated segments separated by conformational kinks. By monitoring the amount of charge-transfer character among neighbor repeating units and the excited-state participation ratio, an average conjugation length of ~8 repeating units is inferred. Interestingly, the same picture holds for interacting chains that visit a conformational space similar to that of isolated chains and feature similar conjugation lengths. There are, however, two major differences between the gas-phase and bulk results:

(i) In the bulk, the conformation of the chain is preserved over a significantly longer time range, typically a few tens of picoseconds, as a result of packing effects (compared to a few picoseconds for isolated chains). This has important consequences for the mechanisms of energy diffusion processes in MEH-PPV. Indeed, the interplay between conformational motion and excitation hopping sets up the overall time scale for energy transport. Do the chains behave as static entities during energy transfer, or in the opposite limiting case, is the hopping gated by fast changes in the conformation of the chains? In a recent paper,<sup>55</sup> experiments were conducted to assess the conformational relaxation rates in small substituted oligo(phenylenevinylene)s while increasing the volume of the side chains and the solvent viscosity. It was concluded that the interpretation of multiexponential fluorescence decays in terms of resonance energy transfer should be revised to include conformational relaxation as an additional process occurring in PPVs bearing side chains. Though our calculations cannot be directly compared to these data (as they are performed in the ground-state

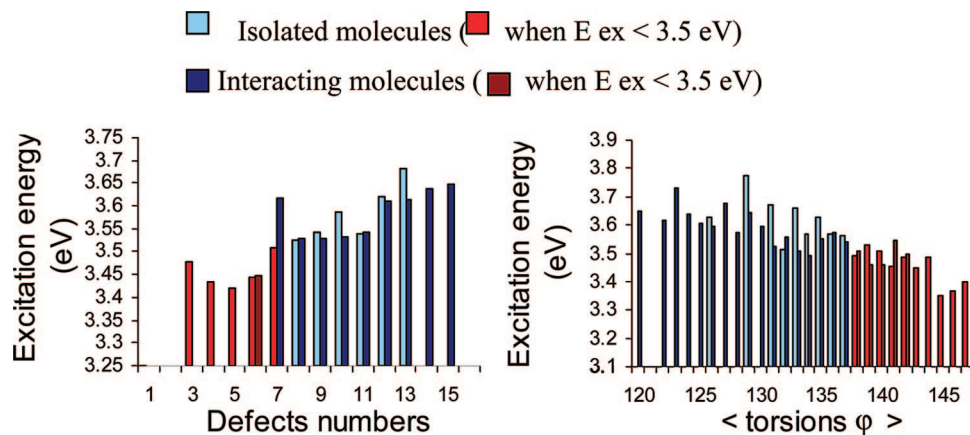


**Figure 13.** Vertical excitation energy as a function of the average torsion angles  $\phi$  (left) and the number of conformational defects (right).

geometry of the isolated and bulk phases), the rapid correlation times extracted from the calculations on isolated chains support this view. In the bulk, however, conformational fluctuations occur on time scales (10–50 ps) that are likely larger than typical energy hopping times (1–10 ps),<sup>56,57</sup> so that a rigid lattice seems to be a reasonable approximation.

(ii) The nonuniform density in the bulk results in the formation of low-energy segments with, on average, more planar configurations. These could account for the “red sites” observed by single molecule spectroscopy on MEH-PPV chains.<sup>15</sup>

Our work provides a first attempt to rationalize within a single theoretical framework the complicated interplay between conformational motion and the nature and dynamics of electronic excitations in conjugated polymers in the gas and bulk phases. We are now extending our investigations to solutions with an emphasis on the impact of solvent polarity, which has been shown to strongly impact the conformation of MEH-PPV chains.<sup>58</sup> Also, the approach used here is based on the combination of a detailed study of the ground-state potential energy surface at the force-field level with vertical electronic excitations using a semiempirical quantum-chemical method. It is well-known that conjugated molecules and polymers are soft materials that can undergo significant geometric relaxation phenomena in the electronic excited state; see, e.g., ref 59. These are currently being implemented in our theoretical formalism. In the specific case of MEH-PPV, though, we do not expect that taking into account excited-state geometric relaxation will significantly impact the overall picture because of similar ground-state and excited-state potential energy surfaces. As a matter of fact, a recent study by Sterpone and Rossky shows that PPV chains have only a slight preference for more planar conformations in the excited state and that this effect is blurred by thermal motions inducing more pronounced out-of-plane deformations in both ground and excited electronic states.<sup>60</sup>

**Acknowledgment.** This work was financially supported by the Belgian National Science Foundation (FNRS FRFC No. 2.4560.00), by the EC STREP project MODECOM (NMP-CT-2006-016434), and by the Belgian Federal Science Policy Office in the framework of the “Pôle d’Attraction Interuniversitaire en Chimie Supramoléculaire et Catalyse Supramoléculaire (PAI 5/3)”. D.B. is a Research Associate of the FNRS. C.D.L. is grateful to FRIA for a doctoral fellowship. J.-C.S.-G. thanks the “Ministerio de Educacion y Ciencia” of Spain (CTQ2007-66461/BQU) for a research contract under the “Ramon y Cajal” program.

## References and Notes

- Chen, L.; Mc Branch, D. W.; Wang, H.-L.; Helgeson, R.; Wudl, F.; Whitten, D. G. *Proc. Natl. Acad. Sci. U.S.A.* **1999**, *96*, 12287.
- Gaylord, B. S.; Heeger, A. J.; Bazan, G. C. *Proc. Natl. Acad. Sci. U.S.A.* **2002**, *99*, 10954.
- Fan, C.; Wang, S.; Hong, J. W.; Bazan, G. C.; Plaxco, K. W.; Heeger, A. J. *Proc. Natl. Acad. Sci. U.S.A.* **2003**, *100*, 6297.
- (a) Van Grondelle, R.; Dekker, J. P.; Gillbro, T.; Sundström, V. *Biochem. Biophys. Acta* **1994**, *1187*, 1. (b) Sundström, V.; Pullerits, T.; Van Grondele, R. *J. J. Phys. Chem. B* **1999**, *103*, 2327.
- Scholes, G. D.; Flemming, G. R. *J. Phys. Chem. B* **2000**, *104*, 1854.
- Nguyen, T. Q.; Kwong, R. C.; Thompson, M. E.; Schwartz, B. J. *Appl. Phys. Lett.* **2000**, *76*, 2454.
- McQuade, D. T.; Pullen, A. E.; Swager, T. M. *Chem. Rev.* **2000**, *100*, 2537.
- Van Averbeke, B.; Beljonne, D.; Hennebicq, E. *Adv. Mater.* **2008**, *18*, 492.
- Hennebicq, E.; Deleener, C.; Bredas, J.-L.; Scholes, G. D.; Beljonne, D. *J. Chem. Phys.* **2006**, *125*, 54901.
- Kwasniewski, S. P.; François, J. P.; Deleuze, M. S. *J. Phys. Chem. A* **2003**, *107*, 5168.
- Liu, L. Y.; Yaron, D.; Sluch, M. I.; Berg, M. A. *J. Phys. Chem. B* **2006**, *110*, 18844.
- Beenken, W. J. D.; Pullerits, T. *J. Phys. Chem. B* **2004**, *108*, 6164.
- Padamanaban, G.; Ramakrishnan, S. *J. Am. Chem. Soc.* **2000**, *122*, 2244.
- (a) Rauscher, U.; Bässler, H.; Bradley, D. D. C.; Hermecke, M. *Phys. Rev. B* **1990**, *42*, 9830. (b) Mollay, B.; Lemme, U.; Kersting, R.; Mahrt, R. F.; Kurz, H.; Kauffmann, H. F.; Bässler, H. *Phys. Rev. B* **1994**, *50*, 10769. (c) Sperling, J.; Milota, F.; Torschanoff, A.; Warmuth, Ch. *J. Chem. Phys.* **2002**, *117*, 10877.
- (a) Hu, D.; Yu, J.; Wong, K.; Bagchi, B.; Rossky, P. J.; Barbara, P. F. *Nature* **2000**, *405*, 1030. (b) Hu, D.; Yu, J.; Wong, K.; Bagchi, B.; Rossky, P. J.; Barbara, P. F. *Science* **2000**, *289*, 1327. (c) Barbara, P. F.; Gesquiere, A. J.; Park, S.-J.; Lee, Y. J. *J. Acc. Chem. Res.* **2005**, *38*, 602.
- (16) Bernius, M. T.; Inbasekaran, M.; O’Brien, J.; Wu, W. *Adv. Mater.* **2000**, *12*, 1737.
- Schwartz, B. *J. Annu. Rev. Phys. Chem.* **2003**, *54*, 141.
- (a) Schindler, F.; Lupton, J. M.; Feldmann, J.; Scherf, U. *Proc. Natl. Acad. Sci. U.S.A.* **2005**, *101*, 14695. (b) Schindler, F.; Lupton, J. M. *ChemPhysChem* **2005**, *6*, 926.
- (19) Lammi, R. K.; Barbara, P. F. *Photochem. Photobiol. Sci.* **2005**, *4*, 95.
- (20) Cornil, J.; Gueli, I.; Dkhissi, A.; Sancho-Garcia, J. C.; Hennebicq, E.; Calbert, J. P.; Lemaire, V.; Beljonne, D.; Brédas, J.-L. *J. Chem. Phys.* **2003**, *118*, 6615.
- (21) Huser, T.; Tan, M.; Rothberg, L. *J. Proc. Natl. Acad. Sci. U.S.A.* **2000**, *97*, 11187.
- (22) Allinger, N. L.; Burkert, U. *Molecular Mechanics*; American Chemical Society: Washington, DC, 1982.
- (23) Ridley, J.; Zerner, M. C. *Theor. Chim. Acta* **1973**, *32*, 111.
- (24) Cerius2, version 4.0, Molecular Simulations Inc, www.msi.com.
- (25) Material Studio, MS Modeling V.3.0.0.0, Accelrys Inc, www.accelrys.com.
- (26) Parr, R. G.; Yang, W. *Density Functional Theory of Atoms and Molecules*; Oxford University Press: New York, 1989.
- (27) www.Gaussian.com.
- (28) Choi, C. H.; Kertesz, M. *J. Phys. Chem. A* **1997**, *101*, 3823.
- (29) Martin, J. M. L.; El-Yazal, J.; François, J.-P. *Mol. Phys.* **1995**, *86*, 1437.
- (30) Becke, A. D. *Phys. Rev. A* **1988**, *38*, 3098.
- (31) Lee, C.; Yang, W.; Parr, R. G. *Phys. Rev. B* **1988**, *37*, 785.
- (32) Vosko, S. H.; Wilk, L.; Nusair, M. *Can. J. Phys.* **1980**, *58*, 1200.
- (33) Becke, A. D. *J. Chem. Phys.* **1993**, *98*, 5648.
- (34) Claes, L.; François, J.-P.; Deleuze, M. S. *Chem. Phys. Lett.* **2001**, *339*, 216.
- (35) Kwasniewski, S. P.; Claes, L.; François, J.-P.; Deleuze, M. S. *J. Chem. Phys.* **2003**, *118*, 7823.
- (36) Van Mourik, T.; Gdanitz, R. J. *J. Chem. Phys.* **2002**, *116*, 9620.
- (37) Toze, J.; Handy, N. C. *J. Chem. Phys.* **1998**, *109*, 10180.
- (38) Casida, M. E.; Casida, K. C.; Salahub, D. R. *Int. J. Quantum Chem.* **1998**, *70*, 933.
- (39) (a) Sancho-Garcia, J. C.; Pérez-Jiménez, A. J. *J. Phys. B* **2002**, *35*, 1509. (b) Sancho-Garcia, J. C. *J. Phys. Chem. A* **2005**, *109*, 3470.
- (40) Choi, C. H.; Kertesz, M. *J. Phys. Chem. A* **1997**, *101*, 3823.
- (41) Rappé, A. K.; Casewit, C. J.; Colwell, K. S.; Goddard, W. A.; Skiff, W. M. *J. Am. Chem. Soc.* **1992**, *114*, 25.
- (42) Bunte, Q. W.; Sun, H. *J. Phys. Chem. B* **2000**, *104*, 2477.
- (43) Traetteberg, M.; Frantsen, E. B.; Mijlhoff, F. C.; Hoekstra, A. J. *Mol. Struct.* **1975**, *2657*.
- (44) Robertson, M.; Woodward, I. *Proc. R. Soc. London, Ser. A* **1937**, *162*, 568.
- (45) Finder, C. J.; Newton, M. G.; Allinger, N. L. *Acta Crystallogr., Sect. B* **1974**, *30*, 411.
- (46) Bouwstra, J. A.; Schouten, A.; Kroon, J. *Acta Crystallogr., Sect. C* **1984**, *40*, 428.
- (47) Hoekstra, H. A.; Meertens, P.; Vos, A. *Acta Crystallogr., Sect. B* **1975**, *31*, 2813.
- (48) Warshel, A. *J. Chem. Phys.* **1975**, *62*, 214.
- (49) Hohneicher, G.; Mueller, M.; Demmer, M.; Lex, J.; Penn, J. H.; Gan, L.-X.; Loesel, P. D. *J. Am. Chem. Soc.* **1988**, *110*, 4483.
- (50) (a) ZOA V3.0, Calbert, J.-Ph. Laboratory for chemistry of Novel Materials, Mons Belgium; see also. (b) Zoyer, E.; Buchacher, P.; Wudl, F.; Cornil, J.; Calbert, J. Ph.; Brédas, J. L.; Leising, G. *J. Chem. Phys.* **2000**, *113*, 10002. (c) Rissler, J.; Bässler, H.; Gebhard, F.; Schwerdtfeger, P. *Phys. Rev. B* **2001**, *64*, 45122.
- (51) (a) Fidder, H.; Knoester, J.; Wiersma, D. A. *J. Chem. Phys.* **1991**, *95*, 7880. (b) Schreiber, M.; Toyozawa, Y. *J. Phys. Soc. Jpn.* **1982**, *51*, 1528.
- (52) Grimm, S.; Tabatabai, D.; Scherer, A.; Michaelis, J.; Frank, I. *J. Phys. Chem. B* **2007**, *111*, 12053.
- (53) Gierschner et al. Manuscript in preparation.
- (54) Dyskra et al. Manuscript in preparation.

- (55) Di Paolo, R. E.; Seixas de Melo, J.; Pina, J.; Burrows, H. D.; Morgado, J.; Maçanita, A. L. *ChemPhysChem* **2007**, *8*, 2657.
- (56) (a) Scheblykin, I. G.; Yartsev, A.; Pullerits, T.; Gulbinas, V; Sundström, V. *J. Phys. Chem. B* **2007**, *111*, 6303. (b) Ruseckas, A.; Wood, P.; Samuel, I. D. W.; Webster, G. R.; Mitchell, W. J.; Burn, P. L.; Sundström, V. *Phys. Rev. B* **2005**, *72*, 115214.
- (57) Yang, X.; Dykstra, T. E.; Scholes, G. D. *Phys. Rev. B* **2005**, *71*, 045203.
- (58) Huser, T.; Yan, M.; Rothberg, L. J. *Proc. Natl. Acad. Sci. U.S.A.* **2000**, *97*, 11187.
- (59) Karaburnaliev, S.; Baumgarten, M.; Tyutyulkov, N.; Müllen, K. *J. Phys. Chem.* **1994**, *98*, 11892.
- (60) Sterpone, F.; Rossky, P. J. *J. Phys. Chem. B* **2008**, *112*, 4983.

JP8029902